Journal of Power Sources 267 (2014) 155–159

Contents lists available at ScienceDirect

Journal of Power Sources

journal homepage: www.elsevier.com/locate/jpowsour

Short communication

Low platinum loading for high temperature proton exchange membrane fuel cell developed by ultrasonic spray coating technique

Huaneng Su, Ting-Chu Jao*, Olivia Barron, Bruno G. Pollet, Sivakumar Pasupathi

HySA Systems Competence Centre, South African Institute for Advanced Materials Chemistry (SAIAMC), University of the Western Cape, Robert Sobukwe Road, Bellville 7535, Cape Town, South Africa

HIGHLIGHTS

- Low Pt loading GDEs were first inspected for HT-PEMFC.
- Four different Pt loadings (from 0.138 to 1.208 mg cm^{-2}) were investigated.
- The optimal Pt loading was found to be 0.350 mg cm^{-2}.
- The peak cathode mass power is as high as 0.967 W mg_{Pt}^{-1}.

ARTICLE INFO

Article history:
Received 24 February 2014
Received in revised form
13 May 2014
Accepted 17 May 2014
Available online 27 May 2014

Keywords:
Low Pt loading
Proton exchange membrane fuel cell
High temperature
Membrane electrode assembly
Poly(2,5-benzimidazole)
Ultrasonic spray coating

ABSTRACT

This paper reports use of an ultrasonic-spray for producing low Pt loadings membrane electrode assemblies (MEAs) with the catalyst coated substrate (CCS) fabrication technique. The main MEA subcomponents (catalyst, membrane and gas diffusion layer (GDL)) are supplied from commercial manufacturers. In this study, high temperature (HT) MEAs with phosphoric acid (PA)-doped poly(2,5-benzimidazole) (AB–PBI) membrane are fabricated and tested under 160 °C, hydrogen and air feed 100 and 250 cc min^{-1} and ambient pressure conditions. Four different Pt loadings (from 0.138 to 1.208 mg cm^{-2}) are investigated in this study. The experiment data are determined by *in-situ* electrochemical methods such as polarization curve, electrochemical impedance spectroscopy (EIS) and cyclic voltammetry (CV). The high Pt loading MEA exhibits higher performance at high voltage operating conditions but lower performances at peak power due to the poor mass transfer. The Pt loading 0.350 mg cm^{-2} GDE performs the peak power density and peak cathode mass power to 0.339 W cm^{-2} and 0.967 W mg_{Pt}^{-1}, respectively. This work presents impressive cathode mass power and high fuel cell performance for high temperature proton exchange membrane fuel cells (HT-PEMFCs) with low Pt loadings.

1. Introduction

Due to the high power density, high efficiency, zero emissions, high-quality power, scalability and fast start-up, proton exchange membrane fuel cells (PEMFCs) are considered as promising future power sources [1].

High temperature proton exchange membrane fuel cell (HT-PEMFC) is a relatively new research area which has gained considerable interest recently with over 2000 research articles published since 2012. Among these researches, phosphoric acid (PA)-doped polybenzimidazole (PBI) system is considered as the most promising candidate for HT-PEMFC with the capability of operating up to 200 °C [2–5]. Important properties, e.g. the proton conductivity of and the conduction mechanism in the membranes [6–11], their mechanical properties and gas permeability as well as the development of membrane electrode assemblies (MEAs) based on this type of membrane and their electrochemical performance at various operating conditions have been studied extensively [4,5,12–15]. The high operating temperature of this PA-doped PBI-based fuel cell system offers several advantages: (i) no need for water management systems, (ii) high tolerance for fuel impurities (up to 3% CO in the fuel stream enabling the use of a simple reformer system), (iii) high quality heat that can be utilized for cogeneration purposes, (iv) simplified Flow Field Plate (FFP) design due to improved transport of vapour water in the structures, (v) minimized BoP requirements in turns allowing simpler system designs [16].

* Corresponding author. Tel./fax: +27 21 959 9310.
E-mail address: s968706@gmail.com (T.-C. Jao).

http://dx.doi.org/10.1016/j.jpowsour.2014.05.086
0378-7753/

MEA is the core component of a PEMFC, which plays an important role in determining the whole cell performance. A MEA is a composite of gas diffusion layer (GDL), catalyst layer (CL) and proton exchange membrane (PEM). Generally, a MEA can be prepared by the three following methods: (i) Catalyst coated membrane (CCM), i.e. CLs were deposited onto a membrane directly, (ii) Decal transfer CCM, i.e. coating CL on a substrate and then transferring the CL onto a membrane, and (iii) Catalyst coated substrate (CCS), which deposits CL on GDL (a GDL with CL is called a gas diffusion electrode (GDE)). A MEA is fabricated by either sandwiching a CCM between two GDLs or sandwiching a PEM between two GDEs.

In a MEA, the electrochemical reaction occurs in the CL and it needs a three-phase boundary (TPB) where the catalyst, electrolyte, and gas are all in physical contact. The amount of TPB strongly affects the fuel cell performance [1,17–19]. The TPB is mainly dominated by the CL deposit method and the properties of the catalyst ink being used, by which the CL properties are determined. Therefore, the CL deposit technique and the formula of the catalyst ink dominate not only the fuel cell performance but also the cost. At present, the Pt loading (both cathode and anode) for HT-PEMFC is normally above 0.7 mg cm^{-2} [3,19–21]. For mass production, the catalyst ink cost is approximately 34% of the total stack cost [22]. Thus, lowering Pt loadings of MEAs is becoming one of the most important issues for PEMFCs [23–28]. For HT-PEMFC based on PA-doped PBI membrane, it is a further challenge because liquid PA in the CLs could make the gas transport difficult and impede the electrode reactions by phosphate anion adsorption on the platinum catalyst [12,13]. This could be the reason why currently no literature were found on preparing low Pt loading MEAs for HT-PEMFC even it has become a hot topic in fuel cell area. Good CL deposit techniques are required to create more available TPB and porous structure to mitigate the effect of PA, thereby reaching satisfactory performance with reduced catalyst loading.

In our previous works [23,28], it was found that the ultrasonic spray method can distribute the catalyst ink evenly leading to high platinum utilization due to the unusual experimental conditions caused by efficient stirring and forced convection in the form of ultrasound, cavitation and enhanced mass transport phenomenon. Consequently, it is expected that this technique possesses the ability to reduce the platinum loading of HT-PEMFC. In this paper, the CCS and ultrasonic spray coating technique were combined to fabricate low Pt GDEs for HT-PEMFC. The resultant MEAs were investigated with air oxidant and at ambient pressure for being consistent with real applications. It should be mentioned that it is the first study of low platinum loading MEAs for HT-PEMFCs.

2. Experimental

2.1. MEA fabrication

Catalyst inks consist of supported catalyst (40 wt% Pt/C, Johnson Matthey HiSpec™ 4000), PVDF solution (5 wt%), DMAc. All the contents were added to a glass vial and mixed using an ultrasonic bath. The PVDF in solid phase of catalyst ink was 15 wt%. The catalyst inks were ultrasonically sprayed onto the GDL (Freudenberg, Germany) as GDE. Run paths were created using the Sono-Tek 'Exacta-coat' ultrasonic spray instrument operating at 120 kHz. The Pt loadings were controlled by the number of passes using a given run path. The finished GDEs were heat-treated at 165 °C oven overnight to evaporate the remaining DMAc. A commercially available poly-(2,5-benzimidazole), also known as the ABPBI membrane, Fumapem AM (Fumatech, Germany) was doped in H_3PO_4 at 85 °C and doping H_3PO_4 level was controlled at 270 ± 10% prior to use. The acid-doping level was defined as the ratio of the "weight of PA doped into the membrane" to the "weight of the membrane before doping with PA".

2.2. Single cell test

Together with two gaskets (~200 μm) made of fluorinated polymer, the MEA was assembled by sandwiching the doped membrane between two GDEs impregnated with PA in a single cell fixture (BalticFuelCells GmbH, Germany) without a preceding hot-pressing step. The cell fixture consists of two graphite plates with single serpentine channels. The active area is about 5 cm^2 (23 mm × 23 mm). Electrical heaters and a thermocouple were embedded into the plates and connected to a Cell Compression Unit (Pragma Industries, France), which controlled the cell temperature at 160 °C and the piston pressure at 2 N mm^{-2} in this study.

The cells were operated in a FuelCon Evaluator C test station (FuelCon, Germany). Pure and dry hydrogen was fed to the anode with flow rates of 100 ml min^{-1}. Dry air was fed to cathode with 250 ml min^{-1}. Both the anode and cathode outlet were ambient pressure. Prior to the recording of the polarization curves, the MEAs were operated at constant load at 0.2 A cm^{-2} overnight for activation. The current–voltage polarization curves were obtained by measuring the voltage with two stepwise increments of current density. The first and second section stepwise from 0 to 0.2 A cm^{-2} and 0.2–2 A cm^{-2} with an interval of 0.01 A cm^{-2} and 0.1 A cm^{-2}, respectively. For protecting MEAs, the polarization test of the second section would be stop automatically when the cell voltage below 0.1 V.

2.3. Electrochemical measurements

Electrochemical impedance spectroscopy (EIS) and cyclic voltammetry (CV) were performed using an Autolab PGSTAT 30 Potentiostat/Galvanostat (Metrohm) equipped with a 20 A booster and a frequency response analysis (FRA) module. Because anode polarization is negligible against to cathode polarization during fuel cell operation, so the anode can be used as the counter electrode and reference electrode. The measurements were carried out at a cell voltage of 0.6 V with an amplitude of 10 mV, and in the frequency range of 0.1 Hz–20 kHz. The impedance data were obtained by calculation and simulation with Autolab Nova software.

Voltammetric measurements, undertaken to study the electrochemical active surface area (EASA), were conducted using dry N_2 at the cathode (working electrode) and dry H_2 at the anode

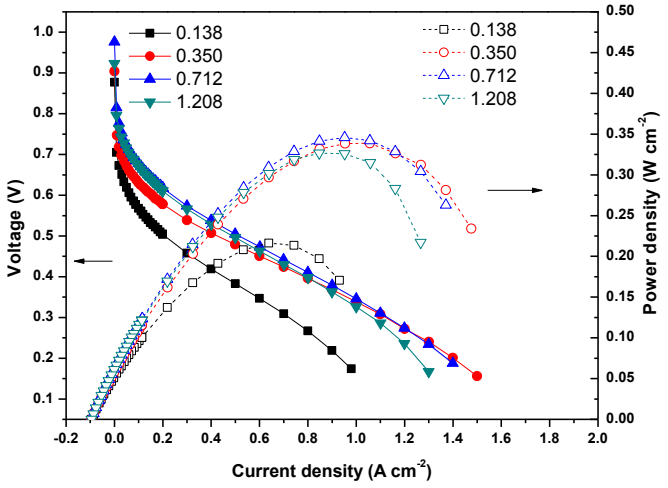

Fig. 1. Polarization curves of the GDEs with different Pt loadings.

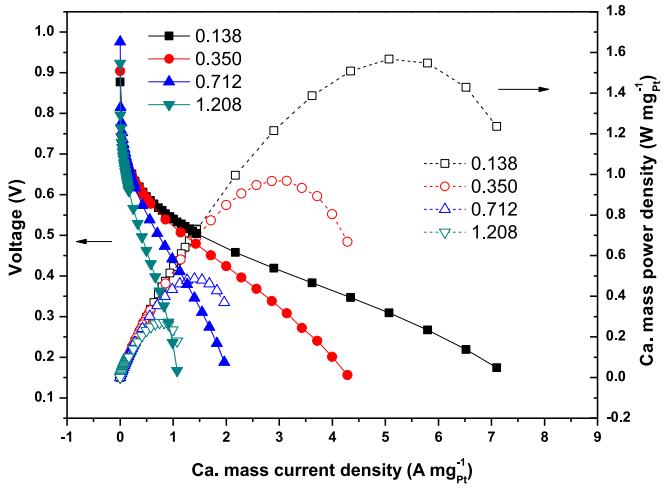

Fig. 2. Cathode mass polarization curves of the GDEs with different Pt loadings.

(counter electrode and reference electrode) at cell operating temperature (~160 °C). Cyclic voltammograms were recorded from 1.2 V to 0.05 V at a scan rate of 0.05 V s^{-1}. The EASA in a CV measurement was calculated using Eq. (1) [19]:

$$\mathrm{EASA} = \frac{100 \cdot A_d}{c \times m \times v} \tag{1}$$

$$A_d = Q_H = \int_{0.05}^{0.4} (i - i_{\mathrm{DL}})\mathrm{d}V \tag{2}$$

The EASA is in m^2 g^{-1}, where A_d is the integral of the hydrogen oxidation desorption peak in the CV curve (in units of AV); c is the coefficient of hydrogen absorbed by platinum (0.21 mC cm^{-2}); m is the amount of platinum at the cathode (in mg); and v is the scanning speed (in mV s^{-1}). The integral for the hydrogen absorption peak is computed in Eq. (2), where i represents the measure current, and i_{DL} is the current due to the electrode double layer charging [19].

3. Results and discussion

3.1. Single cell performance

Fig. 1 shows the polarization curves of the GDEs with different Pt loadings, the legend indicates the Pt loadings of each GDEs and the unit is mg cm^{-2}. The total Pt loading of MEAs is twice of the legend due to the same GDEs were used for anode and cathode. The polarization curves indicate the higher Pt loading performs better at activation domain region but not proportional. The GDE with highest Pt loading of 1.208 mg cm^{-2} shows a faster voltage drop at high current densities (>0.8 A cm^{-2}) compared to other GDEs. Generally, a voltage drop at a high current density is due to mass transport limitations occurring in the electrodes and the membrane. Therefore, the decreased performance of the GDE with the highest Pt loading in the high current density region can be explained by postulating increased mass transport limitations, due to the thicker catalyst layer. The 0.350 mg cm^{-2} GDE performs highest current density at low voltage (<0.3 V) possibly due to the combine of high reaction kinetics and good mass transport resulting from the proper Pt loading. The peak power densities of the GDEs with Pt loadings from low to high are 0.216, 0.339, 0.350 and 0.326 W cm^{-2}, respectively. Except Pt loading 0.138 mg cm^{-2} GDE, the other GDEs had similar peak power densities where the difference was less than 10%.

The cathode mass polarization curves show in Fig. 2, it is the MEAs performance per unit cathode Pt mass. Apparently, the lower Pt loading the higher mass performance because of the performance wasn't increase proportional of Pt loading. The peak mass power densities for the GDEs with Pt loading from low to high were 1.567, 0.967, 0.486 and 0.270 W mg_{Pt}^{-1}, respectively. As discussed above, the Pt loading 0.138 mg cm^{-2} GDE was not in the same level with other GDEs and it performance is not acceptable for real applications. Therefore, the Pt loading 0.350 mg cm^{-2} GDE is the most suitable GDE for low Pt loading MEA of HT-PEMFC because it performance only slightly lower and mass power density is almost twice than 0.712 mg cm^{-2} one.

For completeness, a literature search on current HT-PEMFC performance developed by different techniques was performed, as shown in Table 1. Although many researchers reported the cell performances in their studies on HT-PEMFC, the experimental conditions (e.g. temperature, reactants stoichiometric ratio, Pt loading) were normally varied. It can be seen that PBI and AB–PBI polymer membranes are the most commonly used PEM for HT-PEMFC. Normally, most of these MEAs were operated at around 160 °C and ambient pressure, with an average Pt loadings of ~0.7 mg cm^{-2} on both anode and cathode.

The literature cell performances are typically around 0.5–0.6 W cm^{-2} as maximum power densities, and the peak cathode power can be as high as 1.26 W mg_{Pt}^{-1} [34] when pure oxygen was used as the oxidant. From the point of view of commercialization and real applications, usage of air is more practical to operate PEM fuel cells. When air was used [34], however these values are typically below 0.28 W cm^{-2} and 0.52 W mg_{Pt}^{-1}, respectively. The excellent results of ~0.48 W cm^{-2}

Table 1
Performance comparison of HT-PEMFC developed by different methods.

Coating technique	PEM	Reactants (stoich. ratio at 1 A cm^{-2})	Cell temp. (°C)	Pt loading (mg cm^{-2}) anode, cathode	Peak power density (W cm^{-2})	Peak cathode mass power (W mg_{Pt}^{-1})	Reference
Ultrasonic-spray	AB–PBI	H_2/air (~2.8/3)	160	0.35, 0.35	0.339	0.967	This work
Ultrasonic-spray	AB–PBI	H_2/air (~2.8/3)	160	0.712, 0.712	0.35	0.486	This work
Air-brushing	PBI	H_2/O_2 (~6.5/19)	150	0.5, 0.5	~0.47	~0.95	[29]
Hand-spraying	PBI	H_2/O_2 (~6.2/5)	175	0.6, 0.6	~0.57	~0.95	[30]
Blade coating	AB–PBI	H_2/O_2 (n/a)	150	0.4, 0.55	~0.32	~0.58	[31]
Spraying (double CL)	PBI	H_2/O_2 (n/a)	175	0.4, 0.6	0.56	0.93	[32]
Brushing	AB–PBI	H_2/O_2 (~28/57)	160	0.5, 0.5	~0.43	~0.86	[33]
Brushing	AB–PBI	H_2/O_2 (~28/57)	150	0.75, 0.75	~0.3	~0.4	[19]
Tape-casting	PBI	H_2/O_2 (~2.3/4.6)	200	0.5, 0.5	~0.63	~1.26	[34]
		H_2/air (~2.3/1.9)			~0.26	~0.52	
Automated blade coating	AB–PBI	H_2/air (0.4/0.4)	160	0.8–1.2, 0.8–1.2	~0.28	~0.28	[20]
Commercial MEA	PBI/PPA	H_2/air (1.5/2)	160	1.7 (total)	~0.48	~0.56	[3]
Commercial MEA	PBI/PPA	H_2/air (1.2/2)	160	1.7 (total)	~0.53	~0.62	[21]

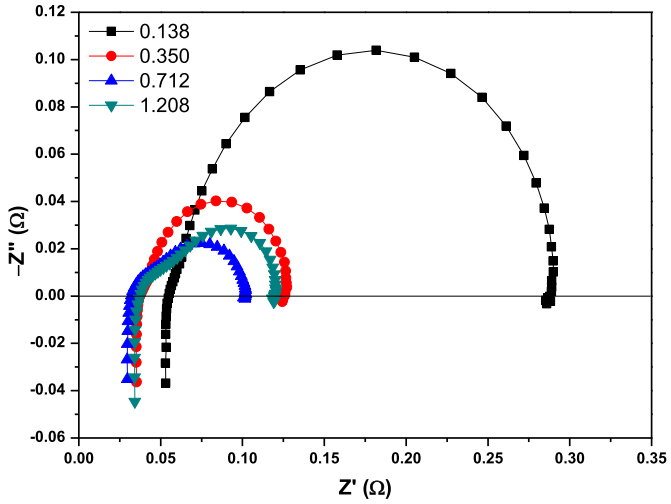

Fig. 3. EIS of the GDEs with different Pt loadings at 0.6 V.

and ~0.53 W cm^{-2} from Zhang et al. [3] and Matar et al. [21] seem only possible due to the use of commercial MEA with the excellent PBI/PPA membrane. With a low Pt loading of 0.35 mg cm^{-2} and the usual operating conditions (~160 °C, H_2/Air, ambient pressure), reaching maximum power density of 0.339 W cm^{-2} and peak cathode mass power of 0.967 W mg$_{Pt}^{-1}$ is therefore considered as a significant achievement in this work.

3.2. Electrochemical properties

EIS was employed to further investigate the electrochemical losses occurring in these GDEs as it provides information on the resistances associated with the voltage-loss mechanisms. The impedance response in the form of Nyquist plots at 0.6 V for the single cell with different GDEs is presented in Fig. 3. It can be seen that only one semicircular arc is discerned in the Nyquist plot, as the electrode process is dominated mainly by the interfacial kinetics of the ORR process. The high-frequency intercept on the real axis represents the total ohmic resistance of the single cell, which is the sum of the ohmic resistances of cell components and the interfacial contact resistances between them. The diameter of the arc is a measure of the charge transfer resistance of the ORR.

Through simulation with Autolab software, the cell resistances (R_Ω) and charge transfer resistances (R_{ct}) of the single cell with the different GDEs can be calculated, and summarized in Table 2. The thicknesses of the GDL (before coating) and the GDEs with different Pt loadings from low to high are ~298.8, ~301.6, ~305.9, ~313.3 and ~323.4 μm, respectively. It can be seen that there is no significant difference in cell ohmic resistance for first three GDEs. However, the GDE with 0.138 mg cm^{-2} Pt loading exhibit a little higher ohmic resistance, which may result from the relatively lower compress ratio and insufficient catalyst amount, leading to an inferior CL/membrane interface contact [35,36]. Meanwhile, the 0.138 mg cm^{-2} GDE had dramatically high charger transfer resistance, suggesting the poor ORR kinetics resulting from insufficient catalyst and phosphate anion adsorption on the Pt sites [37]. The values of R_{ct} for the GDE with 0.35 mg cm^{-2} Pt loading is close to the value of the GDE with highest Pt loading of 1.208 mg cm^{-2}, indicating that this Pt loading is sufficient to obtain an efficient electrochemical active layer for the electrodes prepared by our method. These results are certainly consistent with their performances showed in Fig. 1: the lower the charge transfer resistance, the higher the single cell performance.

Fig. 4 shows the cyclic voltammograms of the GDEs with the different Pt loadings. The corresponding EASAs were calculated from H_2 desorption peak of the voltammogram and the results are also summarized in Table 2. Interestingly, the EASA varied inversely with the Pt loading of the electrode. The GDEs with low Pt loadings (0.138 and 0.350 mg cm^{-2}) showed highest EASA (~30 m^2 g^{-1}) while the lowest EASA (20.47 m^2 g^{-1}) was obtained with the GDE with 1.208 mg cm^{-2} Pt loading. Generally, the EASA depends on the structure of the catalyst layer, as well as the distribution of the electrolyte (i.e. PA) in the CL. Therefore, a low Pt loading electrode means thin catalyst layer, most of the catalyst can be concentrated in the interface between the CL and the electrolyte membrane, resulting in higher Pt utilization. In contrast, thick catalyst layer may suffer with low acid distribution from the membrane, which makes low available Pt catalytic surface in the CL, leading to reduced triple-phase boundaries.

Based on the cell polarization data shown in Fig. 1, the kinetic parameters of the ORR for the GDEs with different Pt loadings were obtained from a Tafel equation:

$$E_{\mathrm{iR-free}} = E_{\mathrm{cell}} + \mathrm{iR} = a - b \log i \tag{3}$$

where E_{cell} is the cell potential, $E_{iR-free}$ is the ohmically corrected cell potential, R is the total cell ohmic resistance accounted for the linear variation of potential with current, a is a constant, which depends on the electrodes and the cell operating conditions, b is the so-called Tafel slope for ORR and i is the current density. Using the value of R determined from high-frequency impedance measurement, the $E_{iR-free}$ Tafel plots [(E_{cell} + iR) vs. log i] were constructed as shown in Fig. 5. The polarization data in the low current density range (<0.1 A cm^{-2}) were fit to Eq. (3) and the Tafel slopes are also summarized in Table 2. The Tafel slopes of these GDEs are found to be 110–127 mV dec^{-1}, which are common for HT-PEMFCs [12,13,38], indicating the same ORR mechanism.

For the estimation of the activities of the GDEs, a simply way is comparing the current generated at a reasonable high potential [39,40]. The current density at 0.7 V (iR free), denoted as $i_{0.7V}$, for each of the GDE is reported in Table 1. As expected, the $i_{0.7V}$ is found to increase generally with increasing amount of Pt. Since catalytic activity is proportional to the EASA, it is meaningful to compare the current density normalized with respect to the EASA rather than electrode geometric area, as shown in Table 2. It can be seen that the GDE with 0.712 mg cm^{-2} Pt loading shows the highest EASA-specific activity, which accords with its performance behaviour in single cell test. However, the specific activities of the electrodes with low and ultra-low Pt loadings are comparable to the GDE with highest Pt loading of 1.208 mg cm^{-2}, implying the possibility of using low Pt loadings for HT-PEMFCs.

Table 2
Electrochemical properties of the GDEs.

Pt loading (mg cm^{-2})	R_Ω at 0.6 V (Ω cm^2)	R_{ct} at 0.6 V (Ω cm^2)	EASA (m^2 g^{-1})	b (V dec^{-1})	$i_{0.7V}$ (mA cm^{-2})	$i_{0.7V}$ (μA cm$^{-2}_{Pt}$)
0.138	0.275	1.175	30.34	0.125	9.99	238.60
0.350	0.185	0.450	30.18	0.111	27.79	263.09
0.712	0.165	0.340	28.38	0.126	74.88	370.57
1.208	0.185	0.415	20.47	0.111	65.69	265.65

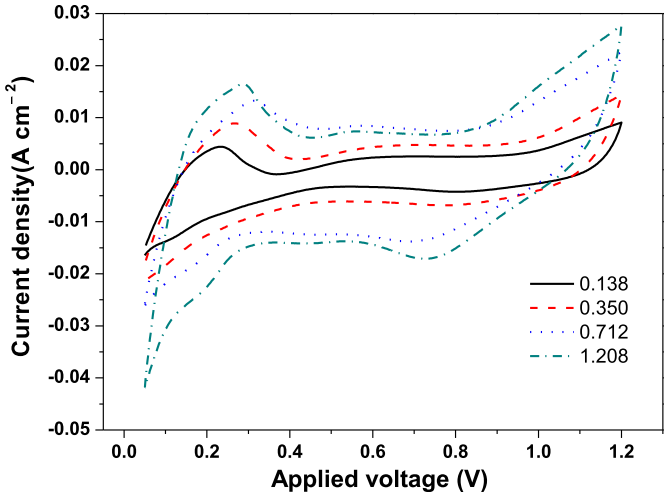

Fig. 4. CV of the GDEs with different Pt loadings.

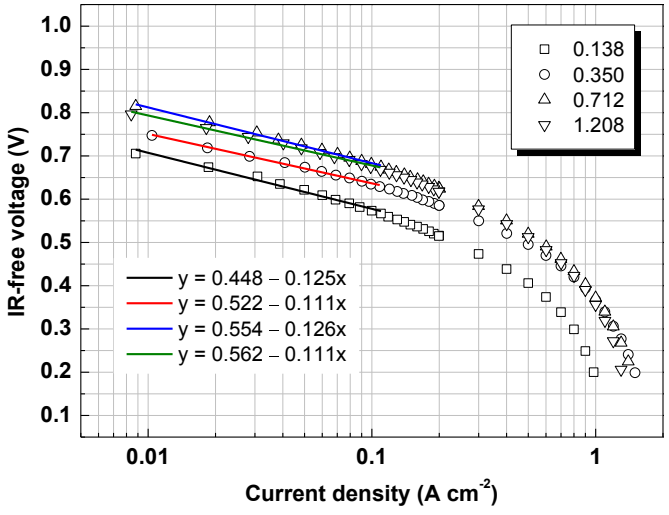

Fig. 5. IR-corrected polarization curves of the GDEs with different Pt loadings.

4. Conclusion

The ultrasonic spray coating technology is very suitable for fabricate high performance low and ultra-low Pt loading MEAs, and it had been demonstrated in low temperature PEMFC. This paper discusses the first use of ultrasonic spray for the fabrication low and ultra-low Pt loading HT-PEMFC MEAs. The result shows Pt loading 0.712 mg cm^{-2} GDE performs the best performance because of highest three boundary phases and electrochemical activity. The Pt loading 0.138 mg cm^{-2} GDE performs the highest mass power density but the performance was much lower than other cases in this study. Thus, the Pt loading 0.350 mg cm^{-2} GDE is the optimal Pt loading for HT-PEMFC with reducing MEA cost purpose. Its peak power density can reach 0.339 W cm^{-2} which is slightly lower than the 0.712 mg cm^{-2} GDE, and peak mass power density can reach 0.967 W mg$_{Pt}^{-1}$ which almost twice than the 0.712 mg cm^{-2} one. The Pt loading 0.350 mg cm^{-2} GDE could have further improvement by adjusting H_3PO_4 doping in GDE, formula and structure etc. This study presents the first results demonstrating high cathode mass power density and fuel cell performance with air oxidant and ambient pressure for HT-PEMFC. Further study will be reported in the future.

Acknowledgements

This work is supported by Hydrogen and Fuel Cell Technologies RDI Programme (HySA), funded by the Department of Science and Technology in South Africa (501100001342) (project KP1-S01).

References

[1] T.-C. Jao, G.-B. Jung, P.-H. Chi, S.-T. Ke, S.-H. Chan, J. Power Sources 196 (2011) 1818–1825.
[2] J.A. Asensio, E.M. Sanchez, P. Gomez-Romero, Chem. Soc. Rev. 39 (2010) 3210–3239.
[3] J. Zhang, Y. Tang, C. Song, J. Zhang, J. Power Sources 172 (2007) 163–171.
[4] Q. Li, J.O. Jensen, R.F. Savinell, N.J. Bjerrum, Prog. Polym. Sci. 34 (2009) 449–477.
[5] J.A. Asensio, P. Gómez-Romero, Fuel Cells 5 (2005) 336–343.
[6] R.H. He, Q.F. Li, G. Xiao, N.J. Bjerrum, J. Memb. Sci. 226 (2003) 169–184.
[7] S.J. Paddison, K.-D. Kreuer, J. Maier, Phys. Chem. Chem. Phys. 8 (2006) 4530–4542.
[8] H. Pu, W.H. Meyer, G. Wegner, J. Polym. Sci. Part B Polym. Phys. 40 (2002) 663–669.
[9] M. Schuster, T. Rager, A. Noda, K.D. Kreuer, J. Maier, Fuel Cells 5 (2005) 355–365.
[10] M.F.H. Schuster, W.H. Meyer, M. Schuster, K.D. Kreuer, Chem. Mater. 16 (2003) 329–337.
[11] H. Steininger, M. Schuster, K. Kreuer, A. Kaltbeitzel, B. Bingöl, W. Meyer, S. Schauff, G. Brunklaus, J. Maier, H. Spiess, Phys. Chem. Chem. Phys. 9 (2007) 1764–1773.
[12] H. Su, T.-C. Jao, S. Pasupathi, B.J. Bladergroen, V. Linkov, B.G. Pollet, J. Power Sources 246 (2014) 63–67.
[13] H. Su, H. Liang, B.J. Bladergroen, V. Linkov, B.G. Pollet, S. Pasupathi, J. Electrochem. Soc. 161 (2014) F506–F512.
[14] H. Su, S. Pasupathi, B. Bladergroen, V. Linkov, B.G. Pollet, Int. J. Hydrogen Energy 38 (2013) 11370–11378.
[15] H. Su, S. Pasupathi, B.J. Bladergroen, V. Linkov, B.G. Pollet, J. Power Sources 242 (2013) 510–519.
[16] S.T. Ali, Q. Li, C. Pan, J.O. Jensen, L.P. Nielsen, P. Møller, Int. J. Hydrogen Energy 36 (2011) 1628–1636.
[17] T.C. Jao, G.B. Jung, S.T. Ke, P.H. Chi, S.H. Chan, Int. J. Energy Res. 35 (2011) 1274–1283.
[18] T.C. Jao, S.T. Ke, P.H. Chi, G.B. Jung, S.H. Chan, Int. J. Hydrogen Energy 35 (2010) 6941–6949.
[19] G.-B. Jung, C.-C. Tseng, C.-C. Yeh, C.-Y. Lin, Int. J. Hydrogen Energy 37 (2012) 13645–13651.
[20] C. Wannek, W. Lehnert, J. Mergel, J. Power Sources 192 (2009) 258–266.
[21] S. Matar, A. Higier, H. Liu, J. Power Sources 195 (2010) 181–184.
[22] B.D. James, J.A. Kalinoski, K.N. Baum, Directed Technologies inc. report, 2010.
[23] T.H. Huang, H.L. Shen, T.C. Jao, F.B. Weng, A. Su, Int. J. Hydrogen Energy 37 (2012) 13872–13879.
[24] M.S. Saha, A.F. Gullá, R.J. Allen, S. Mukerjee, Electrochim. Acta 51 (2006) 4680–4692.
[25] M. Cavarroc, A. Ennadjaoui, M. Mougenot, P. Brault, R. Escalier, Y. Tessier, J. Durand, S. Roualdes, T. Sauvage, C. Coutanceau, Electrochem. Commun. 11 (2009) 859–861.
[26] A.M. Chaparro, B. Gallardo, M.A. Folgado, A.J. Martin, L. Daza, Catal. Today 143 (2009) 237–241.
[27] N. Ramaswamy, T.M. Arruda, W. Wen, N. Hakim, M. Saha, A. Gulla, S. Mukerjee, Electrochim. Acta 54 (2009) 6756–6766.
[28] B. Millington, V. Whipple, B.G. Pollet, J. Power Sources 196 (2011) 8500–8508.
[29] J. Lobato, M.A. Rodrigo, J.J. Linares, K. Scott, J. Power Sources 157 (2006) 284–292.
[30] F. Seland, T. Berning, B. Børresen, R. Tunold, J. Power Sources 160 (2006) 27–36.
[31] J.-H. Kim, H.-J. Kim, T.-H. Lim, H.-I. Lee, J. Power Sources 170 (2007) 275–280.
[32] O.E. Kongstein, T. Berning, B. Børresen, F. Seland, R. Tunold, Energy 32 (2007) 418–422.
[33] A.-L. Ong, G.-B. Jung, C.-C. Wu, W.-M. Yan, Int. J. Hydrogen Energy 35 (2010) 7866–7873.
[34] C. Pan, Q. Li, J.O. Jensen, R. He, L.N. Cleemann, M.S. Nilsson, N.J. Bjerrum, Q. Zeng, J. Power Sources 172 (2007) 278–286.
[35] H. Su, S. Liao, T. Shu, H. Gao, J. Power Sources 195 (2010) 756–761.
[36] H. Su, V. Linkov, B.J. Bladergroen, Int. J. Hydrogen Energy 38 (2013) 9601–9608.
[37] C. Wannek, I. Konradi, J. Mergel, W. Lehnert, Int. J. Hydrogen Energy 34 (2009) 9479–9485.
[38] J.O. Park, K. Kwon, M.D. Cho, S.G. Hong, T.Y. Kim, D.Y. Yoo, J. Electrochem. Soc. 158 (2011) B675–B681.
[39] H.A. Gasteiger, S.S. Kocha, B. Sompalli, F.T. Wagner, Appl. Catal. B 56 (2005) 9–35.
[40] M.S. Saha, D. Malevich, E. Halliop, J.G. Pharoah, B.A. Peppley, K. Karan, J. Electrochem. Soc. 158 (2011) B562–B567.